Surface Plasmon Resonance Based Sensor for Amaranth Detection With Molecularly Imprinted Nanoparticles

Fatma Ozge OZGUR, Duygu ÇIMEN, Adil DENIZLI, and Nilay BERELI*

Department of Chemistry, Hacettepe University, Ankara 06800, Turkey

*Corresponding author: Nilay BERELI E-mail: bereli@hacettepe.edu.tr

Abstract: Amaranth imprinted nanoparticles were prepared by two-phase mini emulsion polymerization of hydroxyethyl methacrylate and ethylene glycol dimethacrylate using acrylamide and methacrylic acid as functional monomers. The amaranth non-imprinted nanoparticle was prepared with the same procedure without using amaranth. Amaranth imprinted and non-imprinted nanoparticles were attached on the chip surface modified with allyl mercaptan. The surfaces of the surface plasmon resonance (SPR) sensor were characterized by the ellipsometry, contact angle, and atomic force microscopy. Amaranth solutions with different concentrations (0.1 mg/mL – 150 mg/mL) were prepared with the pH 7.4 phosphate buffer. The limit of detection and limit of quantification were 0.0180 mg/mL and 0.06 mg/mL, respectively. When the selectivity of the amaranth imprinted SPR sensor was compared with the competing molecules tartrazine and allura red, it was observed that the target molecule amaranth was 5.64 times and 5.18 times more selective than allura red and tartrazine, respectively. The liquid chromatography-mass spectrometry technique (LC-MS) was used for validation studies. According to the results obtained from both SPR sensor and LC-MS analyses, the amaranth recovery (%) from fruit juices was observed between 96% and 99%.

Keywords: Amaranth; surface plasmon resonance; sensors; fruit juice; molecular imprinting

Citation: Fatma Ozge OZGUR, Duygu ÇIMEN, Adil DENIZLI, and Nilay BERELI, "Surface Plasmon Resonance Based Sensor for Amaranth Detection With Molecularly Imprinted Nanoparticles," *Photonic Sensors*, 2023, 13(2): 230201.

1. Introduction

In recent years, the dyes and pigments are frequently used in the food industry to correct color changes that may occur during the production or storage of a food, standardize colors, and provide color to colorless foods [1, 2]. Natural food dyes obtained from natural compounds obtained from plants, fungi or insects, and synthetic dyes as azo, triphenylmethane, xanthene, indigotin, and quinolone group colors are frequently used in the food industry [3]. Azo dyes, one of the synthetic colorants, which have important advantages such as easy dissolution in water, cheap production costs, and high stability against pH, light, temperature, and oxygen, constitute approximately 65% of the commercial paint market. Tartrazine, amaranth, sunset yellow, carmoisine, and allura red are some of the most used azo dyes in the food industry. Amaranth is a reddish dye used to color various foodstuffs and cosmetics [4–6]. Amaranth has been shown to be toxic to human lymphocytes in vitro. In addition, it has been found that the use of drugs such as aspirin in some sensitive people causes reactions such as allergies and asthma [7, 8]. The daily intake (ADI) amount of the amaranth dye in foods has been

Received: 9 March / Revised: 5 September 2022
© The Author(s) 2023. This article is published with open access at Springerlink.com
DOI: 10.1007/s13320-023-0674-0
Article type: Regular

recommended by the World Health Organization (WHO) Expert Committee on Food Additives (JECFA) and the Joint Food and Agriculture Organization (FAO) to be between 0 and 1.5 mg/kg [9].

Various detection techniques such as high performance liquid chromatography-ultra-violet detection, thin layer chromatography, capillary electrophoresis, liquid chromatography-mass spectrometry, and enzyme-linked immunosorbent assay methods are used for the determination of amaranth from foods and beverages [10–15]. Although these techniques are well proven and widely accepted, they also have some disadvantages such as time consuming, technical expertise, extensive sample preparations, and expensive instrument. As a result, it seems extremely necessary to establish a fast, selective, reliable, and cost-effective new method for the determination of colorants used in food products. For this reason, sensor systems have been used for the determination of food dyes in food products in recent years.

The basic principle of the surface plasmon resonance (SPR) sensor is based on optical measurement of changes in the refractive index associated with the binding of target molecules in a sample to biologically recognize molecules immobilized on the SPR sensor surface. The changes to the refractive index enable the desired binding to the SPR sensor surface to occur instantly and the molecular interaction to be observed in real time, quickly and directly. The fast analysis time, label-free and simultaneous detection, high sensitivity, low sample consumption, and repeated use of SPR chips are the main advantages of SPR sensors [16–18]. In addition, there are disadvantages such as non-specific bonding on chip surfaces, expensive chip and instrumentation, and sterile barrier with bonding events [19, 20]. With the use of SPR sensors in food analysis, the number of studies on target analyte determination such as chemical pollutants, pathogens, vitamins, toxins, and allergens is increasing day by day [21–23].

The molecular imprinting technology is a method used in the preparation of polymers with selective and specific recognition sites for the target molecule [24]. In this method based on molecular recognition, cross-linked polymer matrices with specific recognition sites are obtained by polymerization around the target molecule. The cavity formed by the removal of the target molecule from the polymer matrix is complementary to the target molecule in size and shape of functional groups. In this way, polymers with selective recognition sites that can selectively rebind the target molecule are obtained. The most important advantages of molecularly imprinted polymers are that they are easy to prepare, low-cost, reusable, stable, sensitive, and selective to the target molecule [25, 26]. In addition, molecularly imprinted polymers are preferred as a recognition element in many practical applications in the sensor technology, with their properties such as being resistant to acid and base organic solvents, high mechanical properties, and no change in performance when stored for a few years [27, 28].

In this study, amaranth imprinted (MIP) and non-imprinted (NIP) nanoparticles were synthesized and characterization studies were carried out with the electron microscope scanning (SEM) and zeta sizer. Then, amaranth imprinted and non-imprinted nanoparticles were attached on the SPR chip surfaces modified with allyl mercaptan. The surfaces of MIP and NIP SPR sensors were characterized by contact angle measurements, auto-zero imaging ellipsometry, and atomic force microscopy. The kinetic studies were carried out with different aqueous solutions of amaranth in a wide concentration range of 0.1 mg/mL – 150 mg/mL. The real-time detection of amaranth was extensively evaluated with selectivity and reusability analyses. Finally, kinetic analyses were performed with fruit juice samples to show the applicability of the SPR sensor with the liquid chromatography-mass

spectrometry (LC-MS) technique.

2. Experimental section

2.1 Reagents and materials

Amaranth, tartrazin, allura red, polyvinyl alcohol, ammonium persulfate, ethylene glycol dimethacrylate, sodium bicarbonate, sodium bisulfite, sodium dodecyl sulfate, 2-hydroxyethyl methacrylate, methacrylic acid, and acrylamide were obtained from Merck AG (Darm-stadt, Germany) company. Bare gold SPR chip was used in the SPRimager II device and was purchased from GWC Technologies (WI, USA).

2.2 Synthesis and characterization of nanoparticles

Amaranth (AM) was used as the target molecule, and methacrylic acid (MAA) and acrylamide (AAM) were used as monomers for the synthesis of amaranth imprinted (MIP) and non-imprinted (NIP) nanoparticles. Firstly, the pre-polymerization complexes were formed with different molar ratios of MAA and AM monomers by keeping the amount of the target molecule amaranth constant. 20 µL of the prepared pre-polymerization complexes were taken and the total volume was completed to 600 µL with the distilled water. The prepared pre-polymerization complexes were measured at a wavelength of 520 nm in an ultra-violet (UV) spectrophotometer [29]. The obtained absorbance values are shown in Fig. 1. The highest absorbance value was observed in the pre-polymerization complex prepared at the molar ratio AM:MAA:AAM (1:3:1 molar) and used in the synthesis of amaranth imprinted nanoparticles.

The synthesis of MIP and NIP poly(hydroxyethyl methacrylate-methacrylic acid-acrylamide) poly(HEMA-MAA-AAM) nanoparticles was carried out by using the two-phase mini-emulsion polymerization method. 3 different phases such as first aqueous phase, second aqueous phase, and oil phase were prepared for the synthesis of

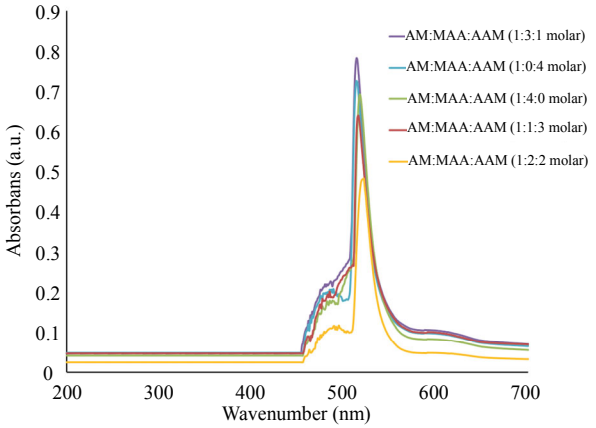

Fig. 1 UV spectrum measurements of AM:MAA:AAM pre-polymerization complexes prepared at different molar ratios.

nanoparticles. The first aqueous phase was the phase prepared by dissolving 15 mg of sodium dodecyl sulfate, 13 mg of sodium bicarbonate, and 100 mg of polyvinyl alcohol in 5 mL of distilled water. 100 mg of sodium dodecyl sulfate and 50 mg of polyvinyl alcohol were dissolved in 100 mL of water and the second aqueous phase was prepared. The oil phase was prepared by homogeneously mixing with 0.600 mL of pre-polymerization complex, 0.25 mL of 2-hydroxyethyl methacrylate, and 1.2 mL of ethylene glycol dimethacrylate for 1 h. After each phase was prepared one by one, the organic phase was slowly added to the first phase and mixed at 6 000 rpm for 30 min in a homogenizer. This prepared polymer mixture was taken in a closed cylindrical reactor and the second aqueous phase was added on it and mixed for another 10 min. Finally, 50 mg of sodium bisulfite and 100 mg of ammonium persulfate initiator pair were added to the prepared polymerization mixture and polymerization was carried out at 500 rpm at 40 ℃ for 24 h. To perform the selectivity experiments for this study, NIP nanoparticles were synthesized using the same polymerization procedure as MIP nanoparticles without using the template molecule amaranth. The surface morphology, size analysis, and distribution of the synthesized nanoparticles were characterized using the zeta sizer device (Nano-ZS, Malvern Instrument, UK), and SEM

(Quanta 400F Field Emission company, USA) device.

2.3 Preparation and characterization studies of SPR sensors

Firstly, the acidic piranha [3:1 (v/v) H_2SO_4:H_2O_2] solution was prepared and 2 mL of this solution were dropped several times on the bare gold SPR chip surface. And then, 4 mL of allyl mercaptan solution were dropped on the SPR chip surface to form thiol (–SH) groups and incubated for 12 h. The SPR chips were washed with an ethanol:water mixture to remove unbound molecules from the surface. 5 μL of MIP and NIP nanoparticles were dropped on the SPR chip surfaces modified with allyl mercaptan and homogeneously coated with the help of a spin coater (Laurell, WS 650Mz-23NPP, USA). The prepared MIP and NIP SPR chips were stabilized under ultraviolet light (100 W, 365 nm) for 20 min and then incubated in an oven at 40 ℃ overnight. A step-by-step pictorial representation of the SPR chip fabrication and experimental setup are shown schematically in Fig. 2.

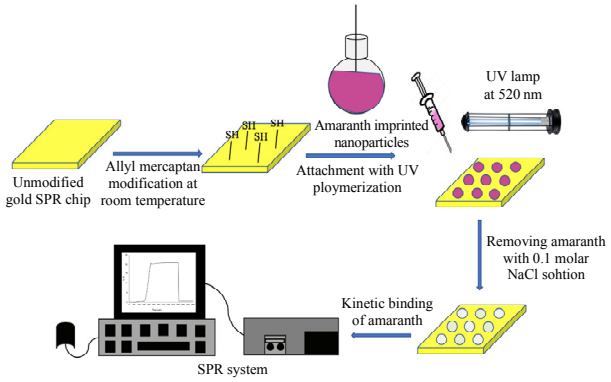

Fig. 2 Step-by-step schematic representation of SPR sensor surface preparation and SPR system.

The surface hydrophilicity, depth, and thickness of the MIP and NIP SPR sensors were examined with three different characterization studies such as contact angle measurements, atomic force microscopy (AFM), and ellipsometer. The wettability and hydrophilicity of the unmodified SPR chip surface and MIP and NIP SPR sensors surfaces were determined using a drop shape analyzer system (Kruss DSA 100, Germany) [30]. For contact angle measurements, the sessile drop method was used by dripping a drop of water on the SPR gold surfaces. 10 photos were taken by dropping water on different parts of the SPR gold surfaces, contact angle measurements were taken for each photo separately and the average of these 10 contact angle values was calculated. The surface morphology of unmodified, MIP and NIP SPR sensors was investigated using AFM (Nanomagnetics Instruments, Oxford, UK) in the tapping mode at a scanning speed of 1 μm/s (resolution: 256×256 pixels) at the 2 μm×2 μm area [31]. The surface thicknesses of the allyl mercaptan modified SPR chip, MIP and NIP SPR sensors, were calculated by averaging 10 measurements with a 20× objective (wavelength: 658 nm and angle of incidence: 62°) using an ellipsometer (Nanofilm EP3, Germany) [21].

2.4 Real-time kinetic analyses

The sensing process in the SPR sensor was the result of optical excitation of a surface plasmon between the dielectric material and a metal with a high conductivity. Kinetic studies for the detection of amaranth from both amaranth aqueous solutions and fruit juice were performed using the SPRimager II (GWC Technologies, Madison, WI, USA) system. The SPRimager system had a Kretschmann configuration and measured the angle of light incident on the SPR surface. In the SPR device, the parallelized p-polarized light from a white light source was passed at a fixed angle through a carbon substrate/prism assembly on a flow cell/metal. Reflected light was collected in a charge coupled device (CCD) camera with a narrow band-pass filter of 830 nm and the obtained data were analyzed with the V++ software package (Digital Optics) [32]. The flow rate of 200 μL/min with the 0.031" ID (Internal diameter) pipe and prism material SF (silicone free) 10 glass (Refractive index, RI=1.720) was used in all kinetic analyses.

Prior to the kinetic analysis for the detection of amaranth, the MIP sensor surface was equilibrated with the pH 7.4 phosphate buffer solution for 3 min. Different amounts of amaranth solutions (0.1 mg/mL – 150 mg/mL) were separately given to the SPR system in the 2 mL solution volume for 7 min. When stable signals were monitored in the SPR system, the 0.1 molar NaCl solution was used as the desorption solution to remove amaranth from the surface for 3 min.

The equilibrium-adsorption-desorption steps were performed in 13 min in all kinetic analyses for the detection of amaranth. The changes in the refractive index (%ΔR) were observed for each analysis separately. In this study, the purpose of using the molecular imprinting technology in the synthesis of nanoparticles was to create specific and selective cavities for that target molecule on the polymer surface [2]. In order to determine the selectivity of amaranth imprinted SPR sensors, kinetic analyses were also performed with non-imprinted SPR sensors. To investigate the selectivity of amaranth imprinted SPR sensors, competitive molecules tartrazine (TA, MW:534.36 g/mol) and allura red (AR, MW: 496.42 g/mol) molecules close to the amaranth (AM, MW: 604.47 g/mol) molecule in both molecular structure and molecular weight were selected. For the detection of amaranth, solutions with the 50 mg/mL concentration were prepared from each competitor molecule and selectivity studies were performed with MIP and NIP SPR sensors. The selectivity coefficient (k) and relative selectivity coefficients (k') were calculated for both MIP and NIP sensors using the following equations obtained from the kinetic analysis [2]:

$$k=\Delta R_{\text{template}}/\Delta R_{\text{competitor}} \quad (1)$$

$$k'=k_{\text{MIP}}/k_{\text{NIP}} . \quad (2)$$

The reusability studies of the amaranth imprinted SPR sensor were performed using the 20 mg/mL amaranth aqueous solution using 4 repeated adsorption-desorption-regeneration cycles. For this purpose, the reusability of the sensor, which was developed using the same chip on the same day, was investigated. In addition, kinetic analyses were performed with the 50 mg/mL amaranth aqueous solution under the same experimental conditions using the same chip at different time intervals (1 month, 2 months, 4 months, and 6 months later). The shelf life and stability of amaranth imprinted SPR sensor, which was prepared at different times, were investigated with the obtained kinetic analysis results.

2.5 Detection of the amaranth from fruit juice

For real sample analysis of the amaranth imprinted SPR sensor, kinetic studies were carried out from real samples using the fruit juice obtained from the market. Firstly, 2 mL of the 18% (v/v) isopropyl alcohol solution with 2 mL of fruit juice were treated for 1 h. The colored juice solution was then placed in a vacuum rotary evaporator and the juice was completely evaporated to obtain a dry amaranth food coloring. The resulting amaranth was transferred to glass bottles to be filtered directly through a 0.45 μm cellulose membrane (CA pore-MFS-13) by adding 3.0 mL of distilled water [33]. 10 mg/mL and 50 mg/mL concentrations of amaranth aqueous solutions were added to the obtained extract from the fruit juice. Kinetic analyses of these prepared solutions were performed with the amaranth imprinted SPR sensor. And then, amaranth amounts in foods were determined using the LC-MS (Thermo Scientific TSQ Quantum Access Triple Quadrupole Device, San Jose, CA, USA) technique for validation studies C18 reverse phase column (2.1 mm × 50 mm, 1.8 μm) was used for the assay analysis of amaranth from the fruit juice. Water:methanol (63:37) v/v and 0.08 molar ammonium acetate:methanol (63:37) v/v solutions and 40 mmolar ammonium acetate solution were used as mobile phase [34]. The dark colored bottles were used during the experiment in the analysis, so that all food samples prepared were not deteriorated by external factors such as light.

3. Experimental results

3.1 Characterization studies of nanoparticles

While the size distribution of amaranth imprinted nanoparticles was measured with the zeta sizer, the surface morphology was visualized by the SEM and it was examined whether molecular imprinting occurred in the polymer. When the size analysis of the synthesized MIP and NIP nanoparticles was performed, the average particle size and polydispersity (PDI) values were observed as 73.92 nm (PDI: 0.139) and 69.81 nm (PDI: 0.137), respectively [Figs. 3(a) and 3(b)]. As seen in Fig. 3(c), the SEM analysis shows that MIP nanoparticles were spherical, homogeneous, and equidimensional. The dimensions of the MIP nanoparticles were found to be approximately 68 nm when examined with the SEM at 150.00 × magnification. According to the zeta sizer and SEM results, it was proved that the synthesized MIP and NIP nanoparticles were successfully synthesized as homogeneous and spherical nanoparticles. The obtained results showed that nano-sized amaranth imprinted particles were successfully produced.

3.2 Characterization of SPR sensor surfaces

To examine the surface properties of the nanoparticle attached on the SPR chip surface, it was characterized using the ellipsometry, AFM, and contact angle measurements. In addition, when the depth and roughness of the SPR sensor surfaces were measured with the AFM and ellipsometer, it was observed that the surface depth was changed and also the unmodified SPR chip surface was coated with imprinted polymer. When the AFM images taken in the tapping mode system were examined, the surface depths of the unmodified SPR chip, and MIP and NIP SPR sensors were found to be 10.03 nm, 41.6 nm, and 37.5 nm, respectively. These results showed that MIP and NIP nanoparticles were homogeneously attached to the chip surface when the unmodified chip surface was compared in Fig. 4.

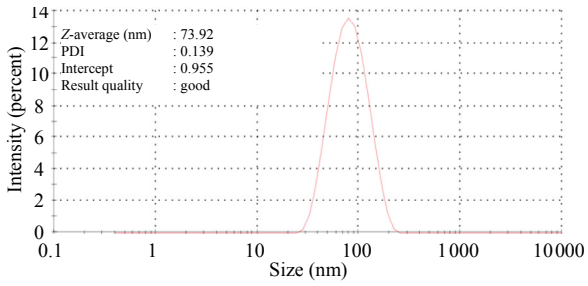

(a)

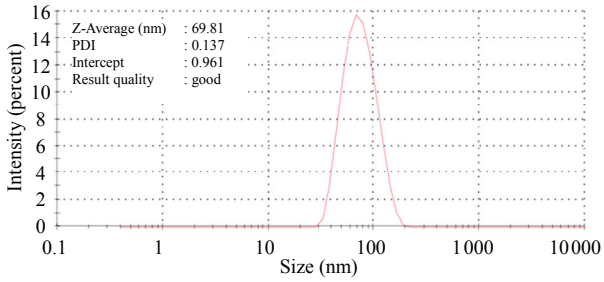

(b)

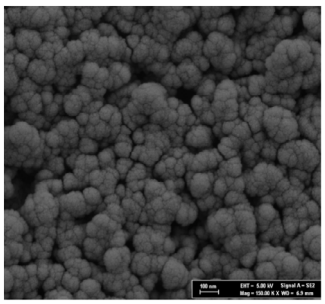

(c)

Fig. 3 Zeta sizer: (a) MIP and (b) NIP nanoparticles; SEM images: (c) MIP nanoparticles.

After attaching with MIP and NIP nanoparticles to SPR chip surfaces modified with allyl mercaptan, the SPR chip surfaces were characterized by the ellipsometry to determine the surface thickness. The thicknesses of the polymers on the MIP and NIP SPR sensors surfaces were calculated as 94.7 nm and 88.1 nm, respectively. The ellipsometre measurement results are shown in Fig. 5. According to the measurement results, it was observed that the nanoparticles on both MIP and NIP SPR sensors surfaces were successfully attached to the chip surface.

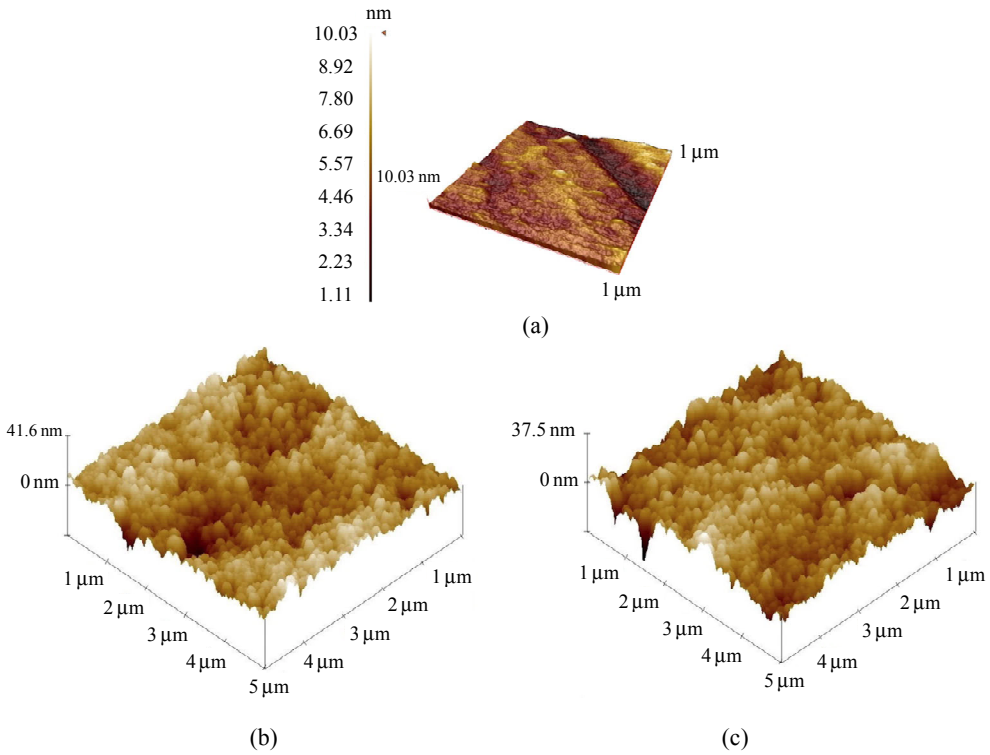

Fig. 4 AFM images: (a) unmodified SPR chip surface; (b) MIP and (c) NIP SPR sensors surfaces.

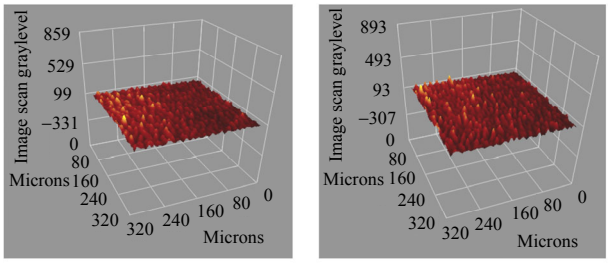

(a) (b)

Fig. 5 Ellipsometer images: (a) MIP and (b) NIP SPR sensors surfaces.

After the attachment of the synthesized nanoparticles on the SPR chip surfaces modified with allyl mercaptan, the contact angle was measured and it was observed that the hydrophilic property of the chip surface increased further due to the hydrophilic property of the imprinted molecule. The wettabilities of the unmodified SPR chip surface and MIP and NIP SPR sensor surfaces were investigated by the sessile drop method and the results are given in Fig. 6. The contact angle values of the unmodified SPR chip surface and MIP and NIP SPR sensors surfaces were obtained as 85.7°, 74.2°, and 70.9°, respectively (Fig. 6). When the contact angles of the unmodified chip surface and the MIP and NIP SPR sensors surfaces were compared, the reason for a decrease in the contact angle was the presence of hydrophilic MAA and AAM monomers in the structure of the synthesized nanoparticles.

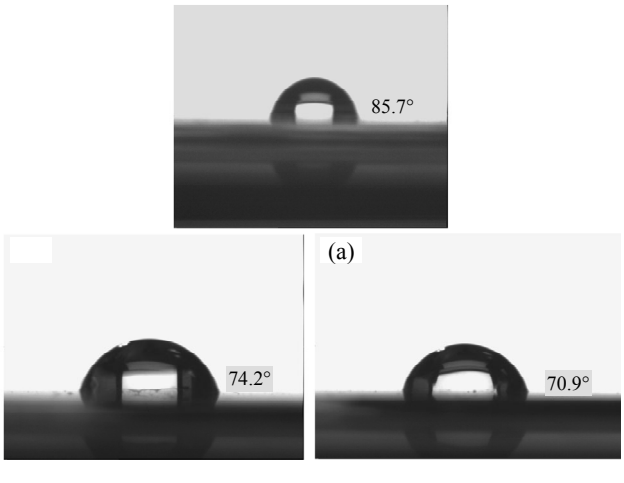

(b) (c)

Fig. 6 Contact angle images: (a) unmodified SPR chip surface; (b) MIP and (c) NIP SPR sensors surfaces.

3.3 Real-time kinetic analysis

All kinetic analyses for the amaranth detection were performed using the SPR imager II device (GWC Technologies, WI, USA). Amaranth solutions were prepared at different concentrations ranging from 0.1 mg/mL to 150 mg/mL in the pH 7.4 phosphate buffer solution. Before starting kinetic analysis, MIP SPR sensors were equilibrated with the pH 7.4 phosphate buffer solution at a flow rate of 200 μL/min for 3 min. And then, kinetic analyses were performed with MIP SPR sensors with aqueous amaranth solutions at different concentrations ranging from 0.1 mg/mL – 150 mg/mL for 7 min. The signals obtained after each kinetic analysis were monitored in real time in the SPR system. Amaranth molecules bound to the SPR sensor surface with the 0.1 molar NaCl desorption solution were removed from the SPR sensor surface for 3 min. For the detection of amaranth, all kinetic analyses were carried out in 13 min as equilibration-adsorption-regeneration cycles. The refractive index (%ΔR) values of the SPR sensor response versus time are shown in Figs. 7(a) and 7(b). It was observed that ΔR values increased with increasing the amaranth concentration.

When the correlation coefficient was examined in the 0.1 mg/mL – 150 mg/mL concentration range for the amaranth imprinted SPR sensor, it is y=0.1359x+ 0.2724 with 99% accurate in Fig. 7(c).

$$\text{Limit of detection (LOD): } 3.3\,S/m \quad (3)$$

$$\text{Limit of quantification (LOQ): } 10\,S/m. \quad (4)$$

LOD and LOQ values were also calculated using the slope of the calibration curve obtained from the kinetic analysis [2]. "S" and "m" represent the standard deviation of the intersection and the slope of the regression line, respectively. LOD and LOQ values for amaranth in the aqueous amaranth solution were 0.018 0 mg/mL and 0.06 mg/mL. Examples of different sensor types for the detection of amaranth in the literature are summarized in Table 1. Although close detection limits and greater detection ranges have been experimented in several studies summarized in Table 1, high selectivity amaranth determination was performed using the molecular imprinting technique in the present study.

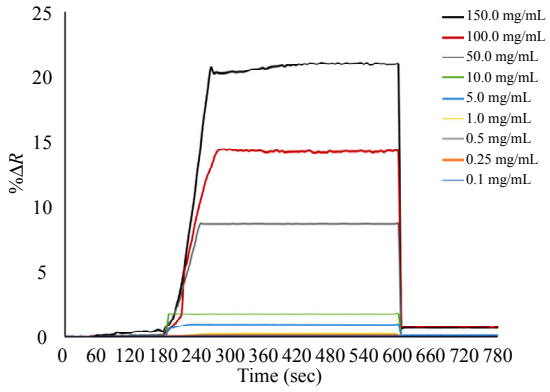

(a)

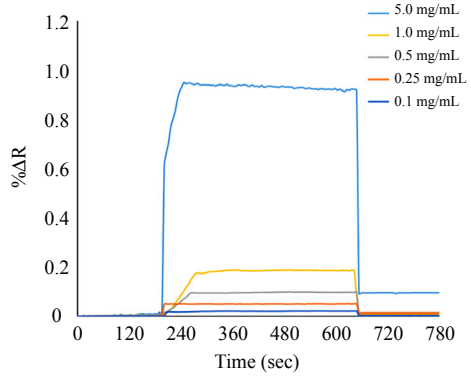

(b)

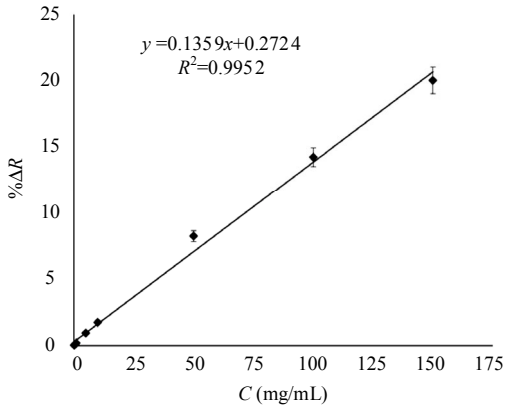

(c)

Fig. 7 Kinetic analysis: amaranth concentration range of (a) between 0.1 mg/mL and 150 mg/mL, (b) between 0.1 mg/mL and 5 mg/mL, and linear regions (c) of the amaranth imprinted SPR sensor aqueous solutions of amaranth at different concentrations.

Table 1 Examples of different sensor studies for detection of amaranth in the beverage sample.

Sensor types	Detection range (mg/mL)	LOD (mg/mL)	Analysis time (min)	Food samples	Ref.
Electrochemical sensor	4.230×10^{-6} – 0.604×10^{-3} 0.241×10^{-3}– 0.01	1.51	20	Watermelon, orange, and grape juice	[35]
Cyclic voltammetry	0.006–0.241	0.604	–	Grape, lemon soda, watermelon, and candy	[36]
Electrochemical sensor	4.83×10^{-6} – 0.725×10^{-3}	1.3×10^{-5}	–	Watermelon, rose and grape flavor	[37]
Electrochemical sensor	0.048 – 217	0.018×10^{-3}	–	Orange and apple juice	[38]
Electrochemical sensor	3.625×10^{-6} – 6.042×10^{-3}	1.2×10^{-6}	–	Soft drink	[39]
Fluorescent sensor	0.4×10^{-6}– 3.5×10^{-6}	0.15×10^{-6}		Candy sample	[40]
Voltammetric sensor	–	0.018×10^{-3}	–	Orange juice	[41]
Electrochemical sensor	0.006–0.06	0.034	–	–	[42]
Electrochemical sensor	1.5×10^{-6}– 0.075×10^{-3}	0.453×10^{-6}	–	Soft drink	[43]
SPR sensor	0.1–150	0.0180	14	Fruit drink	This study

3.4 Selectivity studies

Selectivity is one of the most important and main criteria for molecularly imprinted polymers [23, 26]. Therefore, tartrazine (TA) and allura red (AR) as the food dye used in foods were used to determine the selectivity of the developed sensors. The selectivity of the MIP SPR sensor was tested in comparison with the NIP SPR sensor. Firstly, kinetic analyses were performed by preparing 50 mg/mL AM, AR, and TA solutions to evaluate the selectivity of both the MIP and NIP SPR sensors. And then, solutions of binary AM+AR and AM+TA mixture and ternanry AM+AR+TA mixtures were prepared at the 50 mg/mL concentration and kinetic analyses were performed with both the MIP and NIP SPR sensors. When the selectivity graph, as shown in Fig. 8, was examined, it was seen that the signal response of the MIP SPR sensor to AR and TA molecules was lower than the signal response to the AM. We used the selectivity coefficient (k) and relative efficiency coefficient (k') to calculate the selectivity of MIP and NIP SPR sensors. k' values of the MIP SPR sensor for AM/AR and AM/TA were 5.64 times and 5.18 times, respectively (Table 2). The imprinting factors (IF) for the MIP and NIP SPR sensors were calculated using the $\Delta R_{MIP}/\Delta R_{NIP}$ equation. IFs of the SPR sensor for AM, AR, and TA were 7.77, 1.38, and 1.49, respectively. When the IFs for AM, AR, and TA molecules were compared, the fact that competitor molecules were lower than that of the AM showed that the selectivity of amaranth imprinted nanoparticles significantly increased. It also meant that specific recognition sites on MIP SPR chip surfaces were not suitable for other competing molecules.

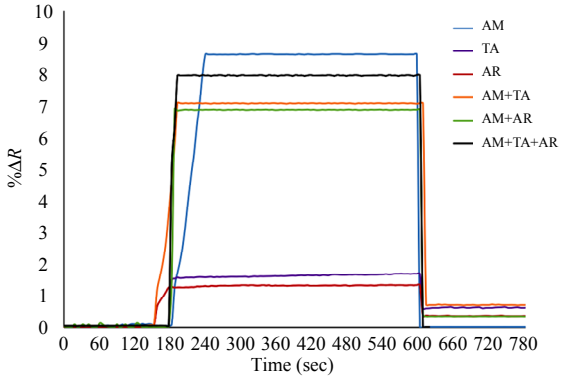

(a)

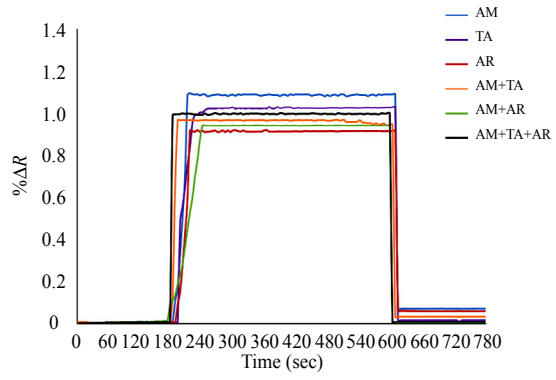

(b)

Fig. 8 Selectivity studies: (a) MIP and (b) NIP SPR sensors.

Table 2 Selectivity parameters.

Molecules	Imprinted		Non-imprinted		
	ΔR	k	ΔR	k	k'
AM	8.63	–	1.11	–	–
AR	1.32	6.54	0.96	1.16	5.64
TA	1.63	5.29	1.09	1.02	5.18
AM+TA	7.08	1.22	1.00	1.11	1.09
AM+AR	6.89	1.25	0.96	1.16	1.08
AM+TA+AR	7.96	1.08	0.94	1.18	0.92

3.5 Reusability studies

Due to the resistance and stableness of the polymeric structure synthesized in SPR sensors prepared by the molecular imprinting method, it has a long shelf life and can be used repeatedly [2]. To examine the reusability of amaranth imprinted SPR sensors, repeated measurements were made 5 times on the same day using the same SPR chip under the same conditions [Fig. 9(a)]. Before starting each kinetic analysis, the SPR sensor was equilibrated with the pH 7.4 phosphate buffer for 3 min. And then, the amaranth solution at the 50 mg/mL concentration was passed through the system for 7 min. Amaranth molecules which were bound to the surface with 0.1 molar NaCl desorption solution were removed from the SPR surface for 3 min.

By repeating the same process 5 times, SPR sensorgrams were taken and the % refractive index of the received sensorgrams is shown in Fig. 9(a). In line with this analysis, which was carried out sequentially in amaranth imprinted SPR sensors, no decrease was observed in the signal and the efficiency value was determined as 95%. After 1 month, 2 months, 4 months, and 6 months, the efficiency and stability of the MIP sensor were tested by performing kinetic analyses at the 50 mg/mL amaranth concentration. After kinetic analysis experiments for the detection of amaranth in different months during a year, it was observed that there was no significant decrease in the responses of the SPR sensor for the detection of amaranth. After 6 months, the efficiency and stability of the MIP SPR sensor were observed that amaranth decreased by 15.62% compared to the initial activity of the MIP SPR sensor [Fig. 9(b)].

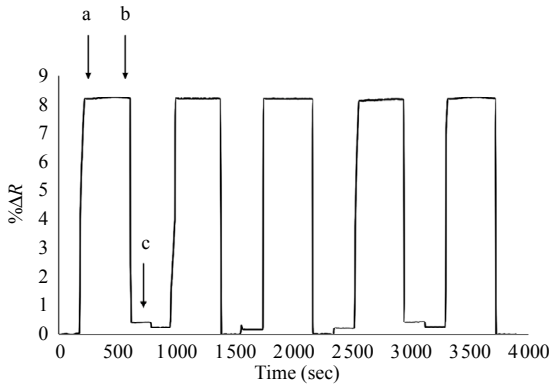

(a)

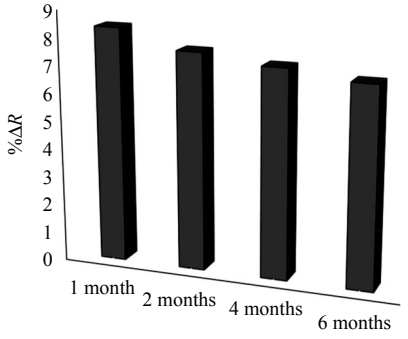

(b)

Fig. 9 Reusability (a) and storage stability (b) studies (a: adsorption; b: desorption; c: regeneration).

3.6 Detection of amaranth from the fruit juice

The applicability of the amaranth imprinted SPR sensor from real samples was carried out by determining amaranth in the fruit juice. Amaranth aqueous solutions prepared at concentrations of 10 mg/mL and 50 mg/mL were spiked to the extraction obtained from the fruit juice. As in the kinetic analysis, the MIP SPR sensor was equilibrated by passing the equilibration buffer (phosphate buffer, pH 7.4) for 3 min. Fruit juice samples spiked at 10 mg/mL and 50 mg/mL amaranth concentrations were given to the SPR system for 7 min. Finally, the 0.1 molar NaCl solution was given to the system and bound amaranth molecules were removed from the MIP

SPR sensor surface for 3 min. In all kinetic analysis steps, the changes in the refractive index (%Δ*R*) of the MIP SPR sensor against time were monitored step by step in Fig. 10. In addition, amaranth amounts in the fruit juice were determined by the LC-MS technique for validation studies. The accuracy and reliability of the MIP SPR sensor for the amaranth detection from the fruit juice were compared with LC-MS results, and the recovery values are given in Table 3. When the results of the kinetic analysis performed with both the MIP SPR sensor and LC-MS were compared with each other, it was seen that the results were compatible with each other. As seen in Table 3, it has been observed that the recoveries were approximately 96% – 99% for both the SPR sensor and LC-MS.

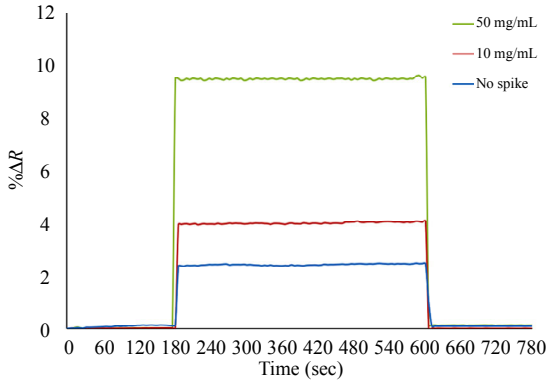

Fig. 10 Real-time kinetic analysis of amaranth in the spiked fruit juice samples.

Table 3 Recoveries of amaranth in fruit juice samples (the number of repetitions in experiments, *n*:3).

Spiked amaranth amount (mg/mL)	Found amaranth (mg/mL)		Recovery (%)	
	SPR	LC-MS	SPR	LC-MS
10	9.70±0.009	9.68±0.006	96.9±0.095	96.85±0.057
50	49.92±0.013	49.90±0.012	99.83±0.026	99.8±0.020

4. Conclusions

Synthetic colorants with the aromatic ring structure and azo groups are frequently used in beverages and their dosages affect human health negatively such as asthma and allergies. In recent years, the detection of the synthetic colorant content has gained importance in the beverage and food industry. In this study, a fast, simple, and inexpensive SPR sensor system was proposed for the selective and sensitive detection of amaranth. The amaranth imprinted SPR sensor was showed a wide linear concentration range (0.1 mg/mL – 150 mg/mL) and a low detection limit (0.0180 mg/mL) for the detection of amaranth. The selectivity of the MIP SPR sensor was tested with competitive molecules such as AR and TA molecules. The selectivity of the MIP SPR sensor to the amaranth molecule was calculated as 5.64 times and 5.18 times higher than those of AR and TA, respectively. These results obtained as a result of selectivity studies showed that the amaranth imprinted SPR sensor had high selectivity for amaranth molecules. When the reusability studies of MIP SPR sensors were performed 5 consecutive kinetic analyses in the same day, it was observed that there was no significant change in the efficiency of the amaranth detection in the MIP SPR sensor response. When the reusability of the amaranth imprinted SPR sensor was examined after 6 months, its efficiency was found to be 84.38%. As a result, it is thought that by integrating amaranth imprinted nanoparticles with SPR sensors, it can be used as a good acceptable measurement method for the future use and development of SPR sensors in the beverage industry in terms of food safety.

Open Access This article is distributed under the terms of the Creative Commons Attribution 4.0 International License (http://creativecommons.org/licenses/by/4.0/), which permits unrestricted use, distribution, and reproduction in any medium, provided you give appropriate credit to the original author(s) and the source, provide a link to the Creative Commons license, and indicate if changes were made.

References

[1] G. T. Sigurdson, P. Tang, and M. M. Giusti, “Natural colorants: Food colorants from natural sources,” *Annual Review of Food Science and Technology*, 2017, 8: 261–280.

[2] N. Bereli, D. Çimen, and A. Denizli, "Optical sensor-based molecular imprinted poly (hydroxyethyl methacrylate-N-methacryloyl-(L)-histidine methyl ester) thin films for determination of tartrazine in fruit juice," *IEEE Sensors Journal*, 2021, 21(12): 13215–13222.

[3] K. Rovina, S. Siddiquee, and S. M. Shaarani, "Toxicology, extraction and analytical methods for determination of amaranth in food and beverage products," *Trends in Food Science and Technology*, 2017, 65: 68–79.

[4] G. G. Bessegato, M. F. Brugnera, and M. V. B. Zanoni, "Electroanalytical sensing of dyes and colorants," *Current Opinion in Electrochemistry*, 2019, 16: 134–142.

[5] P. Mpountoukas, A. Pantazaki, E. Kostareli, P. Christodoulou, D. Kareli, S. Poliliou, *et al.*, "Cytogenetic evaluation and DNA interaction studies of the food colorants amaranth, erythrosine and tartrazine," *Food and Chemical Toxicology*, 2010, 48(10): 2934–2944.

[6] Y. Perdomo, V. Arancibia, O. García-Beltrán, and E. Nagles, "Adsorptive stripping voltammetric determination of amaranth and tartrazine in drinks and gelatins using a screen-printed carbon electrode," *Sensors*, 2017, 17(11): 2665.

[7] K. A. Amin and A. H. Abd Elsttar, "Effect of food azo dyes tartrazine and carmoisine on biochemical parameters related to renal, hepatic function and oxidative stress biomarkers in young male rats," *Food and Chemical Toxicology*, 2010, 48(10): 2994–2999.

[8] S. Tajik, Y. Orooji, F. Karimi, Z. Ghazanfari, H. Beitollahi, M. Shokouhimehr, *et al.*, "High performance of screen-printed graphite electrode modified with Ni-Mo-MOF for voltammetric determination of amaranth," *Journal of Food Measurement and Characterization*, 2021, 15(5): 4617–4622.

[9] M. Wang, Y. Sun, X. Yang, and J. Zhao, "Sensitive determination of Amaranth in drinks by highly dispersed CNT in graphene oxide ''water'' with the aid of small amounts of ionic liquid," *Food Chemistry*, 2015, 179: 318–324.

[10] G. Karanikolopoulos, A. Gerakis, K. Papadopoulou, and I. Mastrantoni, "Determination of synthetic food colorants in fish products by an HPLC-DAD method," *Food Chemistry*, 2015, 177: 197–203.

[11] H. Wu, J. B. Guo, L. M. Du, H. Tian, C. X. Hao, Z. F. Wang, *et al.*, "A rapid shaking-based ionic liquid dispersive liquid phase microextraction for the simultaneous determination of six synthetic food colourants in soft drinks, sugar- and gelatin-based confectionery by high-performance liquid chromatography," *Food Chemistry*, 2013, 141(1): 182–186.

[12] X. H. Chen, Y. G. Zhao, H. Y. Shen, L. X. Zhou, S. D. Pan, and M. C. Jin, "Fast determination of seven synthetic pigments from wine and soft drinks using magnetic dispersive solid-phase extraction followed by liquid chromatography-tandem mass spectrometry," *Journal of Chromatography A*, 2014, 1346: 123–128.

[13] Y. D. Gao, L. Wang, Y. L. Zhang, L. N. Zou, G. P. Li, and B. X. Ye, "Electrochemical behavior of amaranth and its sensitive determination based on Pd-doped polyelectrolyte functionalized graphene modified electrode," *Talanta*, 2017, 168: 146–151.

[14] F. I. Andrade, M. I. F. Guedes, I. G. P. Vieira, F. N. P. Mendes, P. A. S. Rodrigues, C. S.C. Maia, *et al.*, "Determination of synthetic food dyes in commercial soft drinks by TLC and ion-pair HPLC," *Food Chemistry*, 2014, 157: 193–198.

[15] B. Zhang, D. L. Du, M. Meng, S. A. Eremin, V. B. Rybakov, J. H. Zhao, *et al.*, "Determination of amaranth in beverage by indirect competitive enzyme-linked immunosorbent assay (ELISA) based on anti-Amaranth monoclonal antibody," *Food Analytical Methods*, 2014, 7(7): 1498–1505.

[16] C. I. L. Justino, A. C. Freitas, R. Pereira, A. C. Duarte, and T. A. P. Rocha Santos, "Recent developments in recognition elements for chemical sensors and biosensors," *Trends in Analytical Chemistry*, 2015, 68: 2–17.

[17] B. A. Prabowo, A. Purwidyantri, and K. C. Liu, "Surface plasmon resonance optical sensor: a review on light source technology," *Biosensors*, 2018, 8(3): 80.

[18] D. Çimen, N. Bereli, H. Yavuz, and A. Denizli, "Chapter 8: sensors for the detection of food," in *Nanosensors for Environment, Food and Agriculture Vol. 1*. Vineet Kumar, Praveen Guleria Shivendu Ranjan, Nndita Dasgupta, and Eric Lichtfouse, Ed. Switzerland AG: Springer Nature, 2021, pp. 169–182.

[19] J. F. Masson, "Portable and field-deployed surface plasmon resonance and plasmonic sensors," *Analyst*, 2020, 145(11): 3776–3800.

[20] A. K. Srivastava, A. Dev, and S. Karmakar, "Nanosensors and nanobiosensors in food and agriculture," *Environmental Chemistry Letters*, 2018, 16(1): 161–182.

[21] D. Çimen and A. Denizli, "Development of rapid, sensitive, and effective plasmonic nanosensor for the detection of vitamins in infact formula and milk samples," *Photonic Sensors*, 2020, 10(4): 316–332.

[22] S. Faalnouri, D. Çimen, N. Bereli, and A. Denizli, "Surface plasmon resonance nanosensors for detecting amoxicillin in milk samples with amoxicillin imprinted poly(hydroxyethyl methacrylate-N-methacryloyl-(L)-glutamic acid)," *ChemistrySelect*, 2020, 5(15): 4761–4769.

[23] D. Çimen, N. Bereli, and A. Denizli, "Patulin imprinted nanoparticles decorated surface plasmon

resonance chips for patulin detection," *Photonic Sensors*, 2022, 12(2): 117–129.

[24] L. Chen, X. Wang, W. Lu, X. Wu, and J. Li, "Molecular imprinting: Perspectives and applications," *Chemical Society Reviews*, 2016, 45(8): 2137–2211.

[25] A. Rico-Yuste and S. Carrasco, "Molecularly imprinted polymer-based hybrid materials for the development of optical sensors," *Polymers*, 2019, 11(7): 1173.

[26] N. Bereli, D. Çimen, S. Hüseynli, and A. Denizli, "Detection of amoxicillin residues in egg extract with a molecularly imprinted polymer on gold microchip using surface plasmon resonance and quartz crystal microbalance methods," *Journal Food Science*, 2020, 85(12): 4153–4160.

[27] Ş. Çıkrık, D. Çimen, N. Bereli, and A. Denizli, "Preparation of surface plasmon resonance-based nanosensor for curcumin detection," *Turkish Journal of Chemistry*, 2022, 46(1): 14–26.

[28] C. Huang, H. Wang, S. Ma, C. Bo, J. Ou, and B. Gong, "Recent application of molecular imprinting technique in food safety," *Journal of Chromatography A*, 2021, 1657: 462579.

[29] E. M. Elgendy and N. A. Al-Zahrani, "Comparative study of natural and synthetic food additive dye amaranth through photochemical reactions," *Internatıonal Journal of Scıentıfic Research*, 2015, 4: 827–832.

[30] E. Bormashenko, "Contact angles of rotating sessile droplets," *Colloids and Surfaces A: Physicochemical and Engineering Aspects*, 2013, 432: 38–41.

[31] O. Payton, A. R. Champneys, M. E. Homer, L. Picco, and M. J. Miles, "Feedback-induced instability in tapping mode atomic force microscopy: theory and experiment," *Proceedings of the Royal Society A*, 2011, 467(2130): 1801–1822.

[32] M. R. Lockett and L. M. Smith, "Fabrication and characterization of DNA arrays prepared on carbon-on-metal substrates," *Analytical Chemistry*, 2009, 81(15): 6429–6437.

[33] F. I. De Andrade, M. I. F. Guedes, Í. G. P. Vieira, F. N. P. Mendes, P. A. S. Rodrigues, C. S. C. Maia, *et al.*, "Determination of synthetic food dyes in commercial soft drinks by TLC and ion-pair HPLC," *Food Chemistry*, 2014, 157: 193–198.

[34] F. Martin, J. M. Oberson, M. Meschiari, and C. Munari, "Determination of 18 water-soluble artificial dyes by LC-MS in selected matrices," *Food Chemistry*, 2016, 197: 1249–1255.

[35] Y. Wu, G. Li, Y. Tian, J. Feng, J. Xiao, J. Liu, *et al.*, "Electropolymerization of molecularly imprinted polypyrrole film on multiwalled carbon nanotube surface for highly selective and stable determination of carcinogenic amaranth," *Journal of Electroanalytical Chemistry*, 2021, 895: 115494.

[36] Q. He, J. Liu, X. Liu, G. Li, P. Deng, and J. Liang, "Manganese dioxide nanorods/electrochemically reduced graphene oxide nanocomposites modified electrodes for cost-effective and ultrasensitive detection of Amaranth," *Colloids and Surfaces B: Biointerfaces,* 2018, 172: 565–572.

[37] Q. Zhang, W. Cheng, D. Wu, Y. Yang, X. Feng, C. Gao, *et al.*, "An electrochemical method for determination of amaranth in drinks using functionalized graphene oxide/chitosan/ionic liquid nanocomposite supported nanoporous gold," *Food Chemistry*, 2022, 367: 130727.

[38] S. Tajik, H. Beitollahi, H. W. Jang, and M. Shokouhimehr, "A simple and sensitive approach for the electrochemical determination of amaranth by a Pd/GO nanomaterial-modified screen-printed electrode," *RSC Advances*, 2021, 11(1): 278–287.

[39] L. Li, H. Zheng, L. Guo, L. Qu, and L. Yu, "A sensitive and selective molecularly imprinted electrochemical sensor based on Pd-Cu bimetallic alloy functionalized graphene for detection of amaranth in soft drink," *Talanta*, 2019, 197: 68–76.

[40] Y. Li, S. Luo, L. Sun, D. Kong, J. Sheng, K. Wang, *et al.*, "A green, simple, and rapid detection for amaranth in candy samples based on the fluorescence quenching of nitrogen-doped graphene quantum dots," *Food Analytical Methods*, 2019, 12(7): 1658–1665.

[41] N. Nuñez-Dallos, M. A. Macías, O. García-Beltrán, J. A. Calderón, E. Nagles, and J. Hurtado, "Voltammetric determination of amaranth and tartrazine with a new double-stranded copper (I) helicate-single-walled carbon nanotube modified screen printed electrode," *Journal of Electroanalytical Chemistry*, 2018, 822: 95–104.

[42] C. Akkapinyo, K. Subannajui, Y. Poo-Arporn, and R. P. Poo-Arporn, "Disposable electrochemical sensor for food colorants detection by reduced graphene oxide and methionine film modified screen printed carbon electrode," *Molecules*, 2021, 26(8): 2312.

[43] W. Huang, M. Zhang, and W. Hu, "N-methyl-2-pyrrolidone-exfoliated graphene nanosheets as sensitive determination platform for amaranth at the nanomolar level," *Ionics*, 2017, 23: 241–246.